A Multiband RF Antenna Duplexer on CMOS: Design and Performance

Mohyee Mikhemar, *Member, IEEE*, Hooman Darabi, *Senior Member, IEEE*, and Asad A. Abidi, *Fellow, IEEE*

***Abstract*—An RF duplexer has been fabricated on a CMOS IC for use in 3G/4G cellular transceivers. The passive circuit sustains large voltage swings in the transmit path, and isolates the receive path from the transmitter by more than 45 dB across a bandwidth of 200 MHz in 3G/4G bands I, II, III, IV, and IX. A low noise amplifier embedded into the duplexer demonstrates a cascade noise figure of 5 dB with more than 27 dB of gain. The duplexer inserts 2.5 dB of loss between power amplifier and antenna.**

***Index Terms*—Antenna tuning unit, autotransformer, balancing network, bridge network, CMOS, diplexer, duplexer, electrical balance, FDD, full-duplex, hybrid transformer, isolation, noise matching, reciprocal circuit, transmitter leakage, 3G.**

I. Introduction

MULTIBAND operation is today a *de facto* requirement for all commercial cellular handsets. A typical 2G/3G cellular transceiver as shown in Fig. 1 covers seven frequency bands to encompass four 2G bands and three 3G bands. Although the RF transceiver is integrated on a single CMOS chip, it needs four external SAW filters and twelve matching components. While there is progress in miniaturization, such as integrating the two power amplifiers (PA)s for 2G into one module, the numerous off-chip filters and duplexers continue to handicap this multiband approach in cost and area. With the advent of 4G, this approach will likely become impractical.

A multiband transceiver is needed along the lines of Fig. 2, which may be thought of as an antenna-ready radio with everything integrated on a single CMOS chip. It consists of the existing transceiver integrated with a multi-mode multi-band PA, all necessary filters, and duplexers [1]. A multi-mode, multiband power amplifier is in the research phase [2], [3]; a multiband RF filter for 2G operation was demonstrated in [4], [5]; and a multi-band duplexer is now described here.

II. Synthesis of the Multiband Duplexer

The duplexer is a network with three ports to which are connected, respectively, the antenna, the transmitter output, and the receiver input as shown in Fig. 3(a) [6]. For concurrent full-duplex operation, the network should ideally isolate the transmitter (TX) output from the receiver (RX) input; convey the available output power from the PA to the antenna (ANT); and transfer the voltage induced on the antenna to the receiver input with almost no attenuation. The theory of duplexers has been studied extensively, and it is known that the gyrator makes an ideal duplexer with constant driving point resistance at all ports [7].

In 3G wireless systems, the duplexer should isolate the RX from the PA by 50 dB or more to prevent saturation of the receiver or damage to the LNA input. Furthermore, it must be able to withstand TX voltages as large as 15 V. On both these counts, a passive realization seems to be the most promising. An active feedforward cancellation is described in [8], where an LMS adaptive filter produces an out-of-phase replica of the TX waveform that is subtracted from the LNA output, and while this arrangement resembles the isolating function of the duplexer, it is not a substitute.

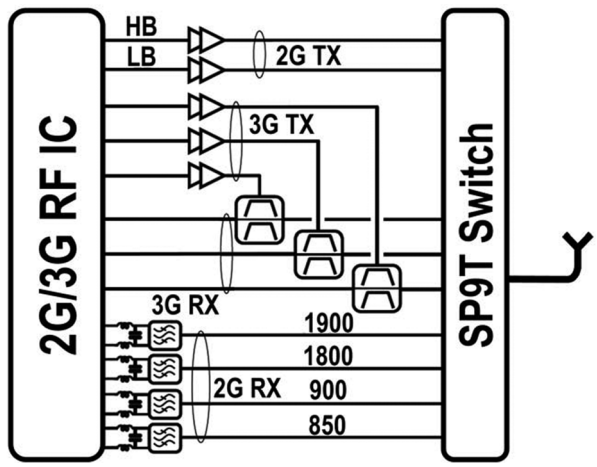

Fig. 1. A simplified block diagram of the RF board in a 2G/3G cellular phone.

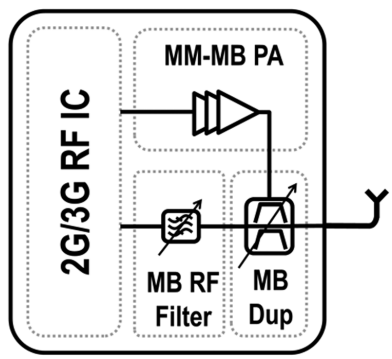

Fig. 2. True multi-band multi-mode radio transceiver.

Manuscript received November 11, 2012; revised April 05, 2013; accepted April 30, 2013. Date of publication June 20, 2013; date of current version August 21, 2013. This paper was approved by Associate Editor Jan Craninckx.

M. Mikhemar was with the Electrical Engineering Department, University of California, Los Angeles, CA 90095 USA, and is now with Broadcom Corporation, Irvine, CA 92617 USA (e-mail: mohyee@broadcom.com).

H. Darabi is with Broadcom Corporation, Irvine, CA 92617 USA.

A. A. Abidi is with the Electrical Engineering Department, University of California, Los Angeles, CA 90095 USA.

Color versions of one or more of the figures in this paper are available online at http://ieeexplore.ieee.org.

Digital Object Identifier 10.1109/JSSC.2013.2264626

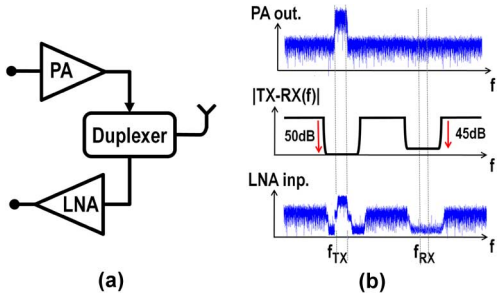

Fig. 3. Duplexer filtering requirements for 3G/4G FDD operation.

How are the three-port duplexers constructed that are used in today's full-duplex mobile telephones? SAW duplexers [9], [10] operate in well-defined non-overlapping narrow bands of frequency for TX and RX, while providing an approximately constant resistance at the TX port. They consist of RX and TX SAW bandpass filters with a steep inter-band transition, so that the RX filter presents a small input reactance across the TX sub-band. An integrated $\lambda/4$ line[1] then transforms this to a large reactance at the TX filter output where the antenna is also connected. Thus, across the TX band, the SAW filter connected to the PA output is terminated essentially only by the antenna impedance.

III. Hybrid Transformer

The hybrid transformer's roots stretch back to the earliest years of telephony [11]–[13]. In the pre-electronic telephone handset it served to isolate the microphone from the earpiece, enabling signals on a pair of wires at each transducer to travel bidirectionally on a two-wire loop to the central office, while suppressing crosstalk from microphone to the headset.

Since the hybrid transformer is a four-port, its analysis can become complicated when tackled without a guiding intuition such as Friedheim's heuristic approach [14], which helps in extracting the circuit's essential properties more straightforwardly.

A hybrid transformer is, at its heart, a bridge circuit with certain useful null, or conjugacy, properties [12], [15]. We start with an analysis of a *symmetrical* hybrid circuit. The *autotransformer hybrid* consists of a coil with a terminal at the center tap as well as at the two ends Fig. 4(a,b) [12], [16]. Ports are defined at the coil's three terminals with respect to a separate common node, or ground, and a fourth (floating) port is defined by the terminals at the coil's two ends. The fourth port could equally well be defined by the terminals of a second, closely coupled, coil which links the magnetic flux of the first coil; this is the classic *hybrid transformer* Fig. 4(c) [12]. A discrete version of the hybrid transformer has recently been demonstrated as an RF duplexer in the 800 MHz band [17]. In this paper we describe the first realization of an autotransformer hybrid constructed on CMOS for RF duplexing in the 2 GHz band.

A. Ideal Hybrid Autotransformer

In keeping with the circuit's eventual use, we label its ports ANT, TX, BAL, and RX (Fig. 5). Assume that equal value resistors R_S are attached between the ANT and BAL ports and common, a resistor $R_{\rm RX}$ is attached across the RX port, and some other $R_{\rm TX}$ across the TX port. Stimuli may be introduced

[1]The physical length of the line is set by the very short acoustic wavelength.

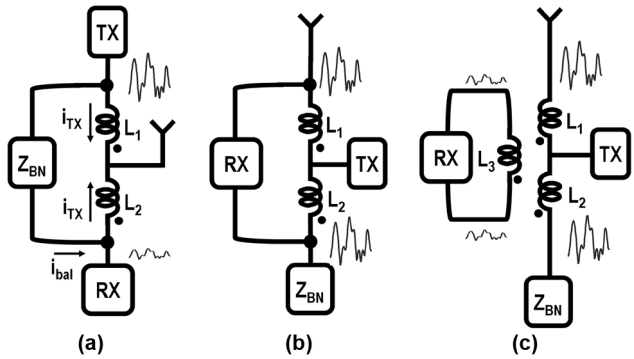

Fig. 4. Duplexer coil configurations a) autotransformer with single-ended RX b) autotransformer with differential RX c) transformer with differential RX and common-mode rejection.

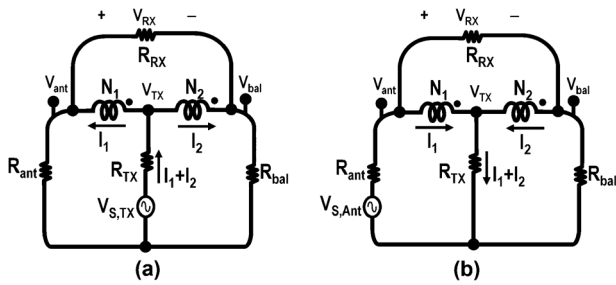

Fig. 5. Hybrid autotransformer model for a) TX mode b) RX mode.

as one or more independent voltage sources in series with the resistor branches, or independent current sources in parallel with them. When subject to multiple stimuli, the response of this linear circuit is the superposition of individual responses.

Suppose a series voltage $V_{\rm TX}$ is inserted in series with the resistor connected to the TX port (Fig. 5(a)). In the spirit of [14], we analyze as follows. The symmetry of the circuit suggests that equal currents flow in the resistors connected to the ports TX and BAL. But since the currents flow from the center tap to the two ends of the coil, they will create equal but opposite magnetic fluxes that cancel to induce zero voltage across the RX port. Since the voltage across the coil is zero, an equal voltage appears across the equal valued resistors in the ANT and BAL branches, verifying the hypothesis that they are carrying equal currents. The circuit must have this as its unique solution, and we have established that the RX port is isolated from the stimulus applied to the TX resistor; in other words, that the TX and RX ports are *conjugate*. This term is a useful reminder that conjugacy is a reciprocal property; we will put it to use in later analysis. When we view the resistors at the ANT and BAL ports as elements in two arms of a bridge, where the two coupled halves of the coil comprise the other two elements, we recognize that isolation arises from the null at the balance of the bridge. In this ideal case the bridge balance depends only on equal impedances being present at the ANT and BAL ports, and therefore TX will remain isolated from RX at all frequencies.

Viewed in a different way, we can say that the hybrid autotransformer isolates TX from RX by presenting the transmit waveform in *common-mode* at the two RX terminals, with respect to the common terminal which we will call ground. And as we will now show, it conveys the antenna voltage to these terminals in *differential mode*, as is desired.

Consider a stimulus voltage in series with $R_{\rm ANT}$ (Fig. 5(b)). Since a bridge circuit is unchanged when its circuit diagram is rotated by 90°, it is reasonable to expect that this port too will have its own conjugate at the BAL port opposite. This is indeed the case, a property called *biconjugacy* [7], [12]. This means that the voltage at the ANT terminal will drop entirely across the coil, leaving zero volts at BAL[2]. Since the coil is center-tapped, KVL in the BAL -TX loop implies that half the voltage must drop across the resistor $R_{\rm TX}$.

Owing to the configuration of resistors and the constraints imposed by an ideal autotransformer, biconjugacy requires that the termination resistances must have specific ratios. When this symmetrical hybrid coil is wound on a core of infinite permeability, the currents entering the dots in the two halves of the coil must cancel, whatever the coil voltage. This means that if a current I flows through $R_{\rm RX}$ it can only complete the loop if a current $2I$ flows through $R_{\rm TX}$ and returns through either the ANT or the BAL terminals. Similarly, when driven from the ANT port, the voltage across $R_{\rm RX}$ is $2\times$ the voltage across $R_{\rm TX}$. It follows that to fulfill these conditions simultaneously, the two resistors must be related as

$$R_{\rm RX} = 4R_{\rm TX} \tag{1}$$

Since $R_{\rm BAL}$ carries no current under ANT stimulus, it might seem that it can take any value; but only a particular value will isolate RX in transmit mode. Indeed several considerations determine the choice of balance resistor $R_{\rm BAL}$:

1) It must balance the bridge so that the TX and RX ports are conjugate.
2) It must enable extraction of all the available power[3] from the voltage source attached to TX.
3) It must consume some small fraction of this power, allowing the rest of it to flow into the ANT port.

In a symmetrical bridge where the hybrid coil is tapped at its center, TX-to-RX isolation requires that $R_{\rm ANT} = R_{\rm BAL}$. This, as we have shown, leads to the constraint that $R_{\rm ANT} = 2R_{\rm TX}$. If this constraint were not met by the inherent values of $R_{\rm ANT}$ (which is usually 50 Ω) and $R_{\rm TX}$ (which is the PA's output resistance), an ideally lossless impedance transformer would be employed to scale $R_{\rm TX}$ until the constraint is met. In the end, though, only half the available power from the transmitter would arrive at the ANT port, while the other half would be lost to the BAL port. In most cases of interest here, this sacrifice in TX power is not acceptable.

Sartori [12] has shown that by shifting the tap off-center, power may be diverted away from the BAL to the ANT port. Our analysis of the asymmetrical circuit derives figures-of-merit that are better suited to the RF application, using arguments that we believe are more fundamental and conceptual.

Since in general $R_{\rm TX} \neq R_{\rm ANT}$, the power transmission from TX to ANT should be characterized by *transducer power gain* ($\mathcal{G}_{tr}$). This is defined as [18], [19]

$$\mathcal{G}_{tr} = \frac{\text{Power delivered to } R_{\rm ANT}}{\text{Power available from source } V_{\rm TX}} \tag{2}$$

where available power from a source is defined in footnote 3. When the transmitter is connected through a lossless matching network to the antenna, $\mathcal{G}_{tr} = 1 = 0$ dB: since no active elements are involved, this is the highest possible power gain. Now when the transmitter couples to the antenna through the hybrid transformer, then owing to loss in $R_{\rm BAL}$ it must be that $\mathcal{G}_{tr} < 1$. When the hybrid is symmetrical and the resistors are related as described above, $\mathcal{G}_{tr} = 0.5 = -3$ dB.

We will now see how asymmetry in the hybrid coil can raise $\mathcal{G}_{tr}$ towards (but never equal to) the maximum value of 1. Let the number of turns in the coil at the ANT end be N_1, and N_2 at the BAL end. To isolate RX from TX, bridge balance requires that

$$\frac{R_{\rm ANT}}{N_1} = \frac{R_{\rm BAL}}{N_2} \tag{3}$$

At balance, the voltage will be equal at all three terminals, ANT, TX, and BAL, which means that the three resistors to ground appear all in parallel. Then to extract the available power from TX it is required that

$$G_{\rm ANT} + G_{\rm BAL} = G_{\rm TX}. \tag{4}$$

where G signifies conductance. Since $R_{\rm ANT}$ is intrinsic to the antenna, which through (3) also determines $R_{\rm BAL}$, the TX PA's source resistance should be scaled through a lossless impedance transformer to satisfy the equality in (4). From now on, $R_{\rm TX}$ will refer to this transformed resistance. With simple analysis, this implies a transducer gain of

$$\mathcal{G}_{tr} = \frac{G_{\rm ANT}}{\frac{G_{\rm TX}}{4}} \left(\frac{G_{\rm TX}}{G_{\rm TX} + G_{\rm ANT} + G_{\rm BAL}} \right)^2 \tag{5}$$

As a check, in the symmetric hybrid where $G_{\rm ANT} = G_{\rm BAL} = G_{\rm TX}/2$ this expression gives the correct value of $\mathcal{G}_{tr} = 0.5$. To apply it to the asymmetric hybrid, we will insert into (5) the balance condition from (3) and the impedance match condition from (4). Then with straightforward manipulations we see that for maximum transducer gain the various conductances must be related as

$$G_{\rm TX} = G_{\rm ANT} \left(1 + \frac{N_1}{N_2} \right) \tag{6}$$

and this maximum gain is

$$\boxed{\mathcal{G}_{tr}(\max) = \frac{1}{1+\left(\frac{N_1}{N_2}\right)} = \mathcal{G}_{avl}(\text{TX} - \text{ANT})} \tag{7}$$

Since TX and ANT ports are individually matched[4], then (7) also specifies the *available gain* ($\mathcal{G}_{avl}$) between these two ports[5]. To reach the maximum available gain of 1 requires that $N_2/N_1 \to \infty$. This stands to reason since in the limit of infinite turns ratio, the condition imposed by (3) will force $G_{\rm BAL} \to 0$ which means that no power will be lost to the now unloaded BAL port.

[2]An ideal transformer can support a voltage across a winding, even when no current flows through it.

[3]Available power from $V_{\rm TX}$ is $(1/4)(V_{\rm TX}^2/R_{\rm TX})$, where $V_{\rm TX}$ is an RMS quantity.

[4]Not necessarily to each other. $R_{\rm ANT}$ is the driving point impedance into the ANT port, and $R_{\rm TX}$ at the TX port, but $R_{\rm ANT} \neq R_{\rm TX}$.

[5]Available gain [20] is the ratio of the available power at the output port to the available power from the source driving the input port.

For good TX efficiency, the circuit designer must select some reasonable turns ratio in the asymmetric hybrid. What will then be the consequence on RX operation? The appropriate figure-of-merit to judge this is *noise factor* at the RX port with the input at the ANT port. The larger the noise factor above 1, the less sensitive is the receiver.

A clear understanding of Friis' definition of noise factor [20] simplifies calculation. In this loaded hybrid coil, as in any reciprocal circuit, the noise factor between two ports is merely the inverse of the available gain from the input to output port. We wish to know the available gain from ANT to RX. Available gain is a property of the Thevenin equivalent of the input source, and of the Thevenin equivalent at the output port with the input source attached: it does *not* depend on the load attached to the output port [19].

If $R_{\rm RX}$ is disconnected from the RX port leaving two open terminals (Fig. 5(b)), then for conjugacy to hold to the \bal port the open circuit voltage between these terminals must be $V_{s,\rm ANT}/2$ (the other half drops across $R_{\rm ANT}$). The impedance between the terminals of the RX port when $V_{s,\rm ANT}=0$ must now be found to complete the Thevenin equivalent. But when RX is made conjugate to TX, to balance the bridge a voltage at TX produces zero voltage across RX, even when the terminals at the RX port are open. It then follows from reciprocity [21, Ch.16, Fig.4.4] that a current source attached to the RX terminals will induce zero current in the TX terminal. Since the current at the TX terminal must be the sum of the currents flowing into the tap from the two parts of the coil, these currents must each be zero. Therefore, the impedance across the RX terminals is $R_{\rm BAL}$ in series with $R_{\rm ANT}$, which is the only available path for current to flow between the terminals.

We now have the necessary information to calculate available gain. The power available from the antenna source $V_{s,\rm ANT}$ (RMS) is

$$P_{avl}(\rm ANT)=\frac{V_{s,\rm ANT}^2}{4R_{\rm ANT}} \tag{8}$$

and from the immediately preceding calculations, the power available at the RX port is

$$\begin{aligned} P_{avl}(\rm RX)&=\frac{V_{s,\rm ANT}^2}{4(R_{\rm BAL}+R_{\rm ANT})}\\ &=\frac{V_{s,\rm ANT}^2}{4}\frac{1}{R_{\rm ANT}\left(1+\frac{N_2}{N_1}\right)} \end{aligned} \tag{9}$$

where we make use of the relation (3) that must be satisfied for conjugacy. Thus the available gain from ANT to RX is given by the ratio

$$\mathcal{G}_{avl}(\rm ANT-RX)=\frac{1}{1+\frac{N_2}{N_1}} \tag{10}$$

and its inverse gives the noise factor from ANT to RX,

$$\boxed{F(\rm ANT-RX)=1+\frac{N_2}{N_1}}. \tag{11}$$

The design tradeoff is now clearly before us. For efficient transmission, the available gain from TX to ANT should approach its maximum of 1, which (7) tells us is a consequence of a large turns ratio $N_2:N_1$. But (11) shows that the noise factor at the RX port rises with this ratio, leading to a worse receiver. The two dependencies are contrary. Why? Because for low loss in transmission the balancing resistor must be chosen very large (and the turns ratio adjusted according to (3)), but then its large noise voltage appears at RX with unity gain, overwhelming the antenna's noise voltage that arrives there accompanying the signal. Noise from the balancing resistor thus degrades the signal-to-noise ratio at RX.

IV. Analysis of On-Chip Duplexer

An asymmetric autotransformer hybrid coil is to be realized on a CMOS chip and evaluated as a wideband duplexer. This coil is a planar inductor tapped at some point in its middle. It is a simpler structure than a classic hybrid transformer, which requires a second closely coupled planar coil that will add to the total parasitic loss through its winding resistance. Electromagnetic field simulations are used to design and optimize the inductor geometry for lowest loss and a sufficiently high self-resonance, and to extract from this geometry an equivalent circuit for simulations.

An on-chip realization will depart in significant ways from the properties of the ideal hybrid coil duplexer that we have analyzed in the previous section.

1) Since there is no magnetic core in the coil, its magnetizing or self-inductance will be determined by the designer to some value on the order of nanohenries; it will certainly *not* be infinite.
2) The ports will be terminated no longer by pure resistances, but by a complex and variable antenna impedance [22] and interconnection parasitics, and in the case of the RX port in our prototype circuit, by a pure capacitance. This will destroy biconjugacy.
3) While the ideal duplexer maintains isolation between TX and RX through bridge balance at all frequencies, in practice due to quite different impedances in the bridge arms (one containing the *off-chip* antenna, the other an *on-chip* balancing network), bridge balance and the ensuing null will typically hold only in a narrow band around one frequency.
4) Transmission from ANT to RX, on the other hand, is a straightforward broadband transfer function independent of a null, that rolls off at high frequencies due to parasitic capacitances.

While in the ideal duplexer simple, well-defined expressions specify the available gain from transmitter to antenna and the associated RX noise factor (and as we will recall, neither of which is 1 in spite of the ideal transformer), resistor losses in the windings of the on-chip coil and other losses will degrade both these quantities by amounts that can only be predicted with accurate field simulations that model the various parasitics.

A. Equivalent Circuit of On-Chip Duplexer

A coil with a center tap (Fig. 6(a)) is described completely, except for parasitic resistance and capacitance, by a T-network of three *uncoupled* inductors (Fig. 6(b)). Two inductors are of value $L_1'=L_1+M$ and $L_2'=L_2+M$, and the third is negative,

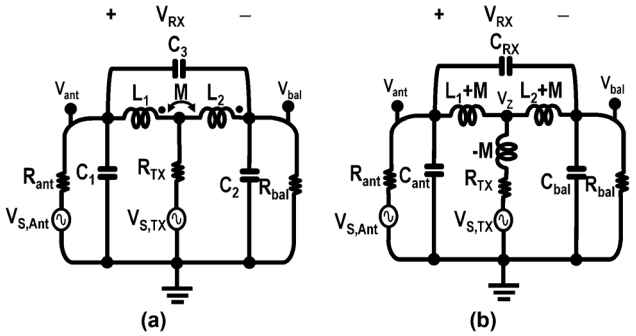

Fig. 6. Hybrid autotransformer model with a) practical autotransformer model b) autotransformer equivalent circuit.

of value $-M$. The signs of M in the three expressions arise from the relative sense of the windings as shown by the dots. L_1 and L_2 is the self-inductance between one of the end terminals of the coil and the center tap, when the terminal at the other end is left floating.

At the RX port, our on-chip duplexer drives a low-noise amplifier whose input is purely capacitive. The loading effect is modelled by two equal capacitors connected from the ANT and the BAL terminals to ground. The antenna attaches to the chip through a bonding pad, whose capacitance C_{pad} appears in parallel. The loss resistance and capacitance to substrate of the on-chip coil are found to have only a small effect, and are ignored.

This simple circuit is good enough to predict the antenna-to-RX transmission function, whose analysis now follows. But the TX to RX isolation analyzed in the subsequent section depends on bridge balance, which is sensitive to small variations in the two bridge arms. Then the equivalent circuit must be supplemented, as we show in Section V-C, with stray inductances and other parasitic elements.

B. Antenna-to-RX Transmission

Fig. 6(b) shows the equivalent circuit that gives the transfer function from the antenna, which is modelled nominally as a 50 Ω voltage source, to the RX port whose open circuit voltage appears at the gates of two FETs. Since this circuit must also isolate the RX port from the transmitter, bridge balance requires that the admittances of the branches on the ANT and BAL ports are in the same ratio as $k \triangleq L_2' : L_1'$, which we call the *skew factor* of the asymmetric hybrid autotransformer. In practice this constraint is satisfied at the BAL port by choosing $R_{\rm BAL} = kR_{\rm ANT}$. When the antenna and interconnect are modelled as a shunt GC network at the duplexer's ANT port, a binary capacitor array in parallel with $R_{\rm BAL}$ to obtain balance by adjusting $C_{\rm BAL} = C_{\rm ANT}/k$,

When the antenna appears inductive as electrically small antennas will, the inductance is tuned with a second capacitor array attached to the ANT port; otherwise an inductor array would be needed at the BAL port, which is impractical. The loading effect of LNA input capacitance is dealt with in a later section. The analysis that follows uses theorems of reciprocity and source shifting [23], but because of limitations of space the steps cannot be included here. It concludes with

$$V_{\rm RX} = \frac{1}{1 + jR_{\rm ANT}\left(\omega C_1 - \frac{1}{\omega L_1'}\right)} V_{s,\rm ANT} \qquad (12)$$

where C_1 is the total capacitance at the ANT port. This is the bandpass transfer function of an LCR resonant circuit, with a peak value of 1 at its resonant frequency $\omega_0 = 1/\sqrt{(L_1' C_1)}$. The coil inductance should be chosen so that this resonant frequency is centered roughly on the band of interest, 2 GHz in our case. At a few GHz, $\sqrt{(L_1'/C_1)} \approx 50\ \Omega$ which means that the quality factor of the resonant circuit is roughly 1 and the transfer function presents a very broad peak with no need for accurate tuning. This is a good approximation to the ideal autotransformer, whose transfer function is 1 at all frequencies.

This hybrid coil is not biconjugate, because its RX port is terminated by a capacitor, not by the resistor specified in (1). Therefore, the driving point impedance at the ANT port is a frequency-dependent complex quantity. We show in Section V-B that it is in fact a constant resistor over the frequencies of interest with a very small reactive part. Section VI presents simulations and measurements of the reflection coefficient at this driving point.

C. TX-to-RX Isolation

The duplexer relies entirely on the null arising from bridge balance to isolate the RX port from the power amplifier that drives the TX port. Consequently, small amounts of imbalance can cause an unacceptable feedthrough. Therefore, great care must go into balancing the two arms of the duplexer over a frequency range that spans the transmit *as well as* the receive bands, since the phase noise spectral tail of the large transmitted signal falls in the receive band and raises the noise floor.

Unbalance in the duplexer bridge arms arises mainly from unpredictable antenna impedance and interconnect cables. Parasitics of connection to and from the chip will play a smaller role. The duplexer is a single tapped planar coil, but since the tap is off-center, the inductance of the two coil segments, L_1' and L_2', must be found accurately from electromagnetic simulations or from experimental characterization of the coil as a two-port network. Parasitic capacitance to substrate will produce frequency dependence in L_1' and L_2'.

Let $Y_{\rm ANT}(\omega) = G_{\rm ANT}(\omega) + jB_{\rm ANT}(\omega)$ signify the Norton equivalent admittance connected to the ANT port, and $Y_{\rm BAL}(\omega) = G_{\rm BAL}(\omega) + jB_{\rm BAL}(\omega)$ the admittance at the balance port. In our circuit the balance network is a digitally selected array of resistors in shunt with a capacitor array, and when inductance to the ground plane is included even $G_{\rm BAL}$ will acquire a small frequency dependence. Isolation from TX to RX requires the following two conditions to hold:

1) At a given transmit carrier frequency $f_{\rm TX}$, there exists a digital selection for $Y_{\rm BAL}$ that will force $|V_{\rm RX}/V_{\rm TX}|(f_{\rm TX}) \leq \epsilon$, where $\epsilon \ll 1$ is the attenuation necessary to provide the desired isolation.
2) If at the same time the receiver is tuned to a carrier frequency $f_{\rm RX}$, then $|V_{\rm RX}/V_{\rm TX}|(f_{\rm RX}) \leq \epsilon$ there also.

The first condition amounts to determining the balance network's ability to reach a null, given spreads in the antenna impedance; and the second condition specifies that the null must attenuate over a wide enough bandwidth to encompass both transmit and receive frequencies. We will deal with these requirements one at a time.

1) Isolation in TX Band: In the manner of (3), the balancing conductance must follow the relation

$$G_{\rm ANT}L_1' = G_{\rm BAL}L_2' \tag{13}$$

To account for variations in the antenna conductance, $G_{\rm BAL}$ must be made adjustable through an array of trimming resistors. This specifies a certain *range* and *resolution*. Range must be wide enough to encompass the full spread of $G_{\rm ANT}$, while resolution limits how small the attenuation ϵ can be. In an array of resistors, range and resolution together will dictate the number of bits.

$C_{\rm ANT}$ arises from antenna reactance, cables, connectors, board traces, the chip package and the LNA, and must be compensated in the balance network by a digitally trimmable capacitance (Fig. 6(b)) obeying the inverse relation,

$$\frac{C_{\rm ANT}}{L_2'} = \frac{C_{\rm BAL}}{L_1'} \tag{14}$$

If this were a complete description, then with sufficient resolution in the shunt GC network the duplexer could be balanced to isolate TX from RX over *all* frequencies. But the model is inadequate for two reasons. First, reflections from nearby objects will cause the antenna to appear reactive as well as (radiation) resistive, and what is worse, its reactance will change as the mobile wireless device moves in its environment [22]. If this is to be balanced by a shunt $G-C$ network, then, in general, the variable span of $R_{\rm BAL}$ and $C_{\rm BAL}$ must be widened to cover likely eventualities.

Today's transceivers employ an antenna tuning unit (ATU) that estimates and tracks the changing impedance by measuring the VSWR in the antenna feed cable. The ATU has been a subject of research for many years [24], [25], and has matured to the point today [26] that it is used in mass-produced handsets to adjust antenna VSWR to 2:1 or less at all times, thus lowering the average PA current drain. We will show later how the balance network as realized on our prototype is good enough to give the desired isolation in a mobile handset, *provided* a state-of-the-art commercial ATU is present on the antenna side of the duplexer[6].

2) Isolation in RX Band: The bridge will balance exactly at only one frequency because the antenna-side admittance comprises, in general, two frequency-dependent terms $G_{\rm ANT}(\omega) + jB_{\rm ANT}(\omega)$. However, it can continue to provide useful isolation over a bandwidth of tens of MHz or more surrounding the null frequency. A key aspect of design is to predict this bandwidth. Parasitic reactances such as bondwire inductance that appear in the balance network will introduce a frequency dependency in the real and imaginary parts of the balancing admittance, i.e. $Y_{\rm BAL}(\omega) = G_{\rm BAL}(\omega) + jB_{\rm BAL}(\omega)$. These various considerations determine the *isolation bandwidth* that is finally achieved.

The following analysis shows a method to estimate this bandwidth. Ignoring some large terms that change slowly with frequency, the TX to RX transfer function is given to within an order of magnitude by

$$\frac{V_{\rm RX}}{V_{\rm TX}}(\omega) \sim j\omega L_1' Y_{\rm ANT}(j\omega) - j\omega L_2' Y_{\rm BAL}(j\omega) \tag{15}$$

Suppose that under digital control, $Y_{\rm BAL} = G_{\rm BAL} + jB_{\rm BAL}$ has enough range that at a frequency ω_0 close to a wireless channel of interest, it can make this transfer function zero[7]. The question is: as frequency is now swept but the control words are frozen, how rapidly does the transfer function depart from zero? Or, more precisely, given some $\epsilon \ll 1$, over what frequency interval surrounding ω_0 is the magnitude of the right-hand side of (15) less than ϵ?

This interval will always be small compared to ω_0. So using a series expansion around ω_0 and retaining only the first term,

$$\frac{G_{\rm ANT}}{kG_{\rm BAL}}(\omega_0+\Delta\omega) \simeq 1 + \frac{d}{d\omega}\frac{G_{\rm ANT}}{G_{\rm BAL}}(\omega)\bigg|_{\omega_0}\frac{\Delta\omega}{k} \tag{16}$$

The same linear approximation will apply to the imaginary parts of admittance, $B_{\rm ANT}$ and $B_{\rm BAL}$. Then, in the vicinity of ω_0, (15)simplifies to

$$\frac{V_{\rm RX}}{V_{\rm TX}}(\omega_0+\Delta\omega) \sim \omega_0 L_1' \left(G_{\rm BAL}(\omega_0)\frac{d}{d\omega}\frac{G_{\rm ANT}}{G_{\rm BAL}}(\omega)\bigg|_{\omega_0} + jB_{\rm BAL}(\omega_0)\frac{d}{d\omega}\frac{B_{\rm ANT}}{B_{\rm BAL}}(\omega)\bigg|_{\omega_0}\right)\Delta\omega \tag{17}$$

The isolation to RX worsens linearly with frequency offset, at a rate set by the frequency derivative of the ratio of the real parts and the ratio of the imaginary parts of the admittances at the ANT and BAL ports. If these ratios are constant with frequency, that is, if the network at the BAL port is an admittance-scaled replica by k of the network on the ANT port, the null will hold for all frequencies. Since it is almost impossible to make these two networks identical, both derivatives of ratios in (17) must be kept small by careful design if we are seeking a large attenuation across a useful bandwidth[8]. We will use this expression to predict the isolation bandwidth in our experimental prototype, and show that it is close to measurement.

[6]This is not a weakness of this RF duplexer, but is inherent in any method of isolation that relies on balancing a bridge. The most widespread use of the hybrid transformer to date was in pre-electronic telephone sets, where a temperature-dependent resistor (varistor) in the balance network adapts to the typically large spreads in resistance of incoming loops [13]

[7]Without well-thought out networks attached to the BAL port and a capacitive trim network at the ANT port, it may be impossible in practice to reach the null condition when parasitic elements are included.

[8]For a correct understanding of this null, it should be noted that the s-domain transfer function from V_{TX} to V_{RX} contains a pair of complex conjugate poles that are found by replacing $j\omega$ in (12) by the complex frequency s, as well as a pair of complex conjugate zeros. With sinusoidal stimulus, if the zeros lie on the $j\omega$-axis of the s-plane a true null will be observed. However, if the zeros lie less than a distance ϵ away from the axis, while a null is not obtained the desired attenuation is seen over some non-zero bandwidth.

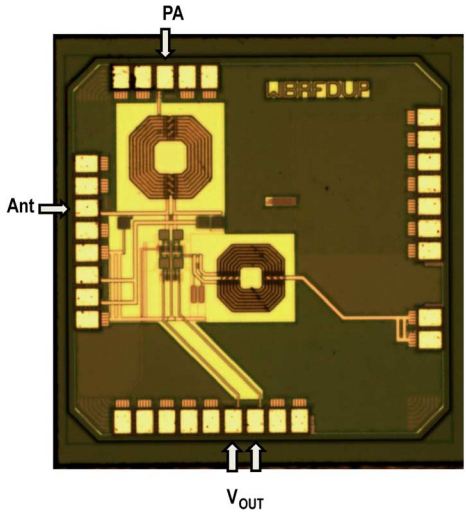

Fig. 7. Chip micrograph of the CMOS duplexer.

D. Figures of Merit for Practical Duplexer

When the two segments of the autotransformer are closely coupled, that is, when at the frequencies of operation,

$$\omega\left(\frac{L_1L_2-M^2}{L_1+L_2+2M}\right)\ll\frac{R_{\rm ANT}}{1+\frac{L_1'}{L_2'}}$$

the expressions for TX -to-ANT gain (7) and for ANT-to-RX noise factor (11) in the ideal transformer change as follows in the practical realization:

$$\mathcal{G}_{avl}(\mathrm{TX}-\mathrm{ANT})\simeq\frac{1}{1+\left(\frac{L_1'}{L_2'}\right)};$$
$$F(\mathrm{ANT}-\mathrm{RX})\simeq 1+\frac{L_2'}{L_1'} \tag{18}$$

The matching network at the PA attached to the TX port remains almost the same as it would be for an ideal hybrid autotransformer.

V. Details of Experimental Prototype

The prototype test circuit was realized in a 65 nm CMOS technology. The circuit consists of a hybrid autotransformer, a low-noise amplifier attached to its RX port, a digitally controlled balancing network on the BAL port, and a binary weighted array of small capacitors on the ANT port. The chip micrograph is shown in Fig. 7. The duplexer occupies an area of $0.2\ \mathrm{mm}^2$ dominated by the two inductors. The large inductor on top is the duplexer autotransformer; the other inductor is the LNA load.

A. Design of Tapped Hybrid Coil

The design of a duplexer that spans multiple frequency bands requires careful modelling and optimization of the on-chip autotransformer. In this instance, electromagnetic simulations of a symmetric planar spiral autotransformer with a total inductance of about 10 nH, chosen to center its operation at 1.5 GHz, predict $\mathcal{G}_{tr}=-3.4$ dB in both TX and RX directions. The 0.4 dB beyond the theoretical -3 dB (see (18)) is due to losses in the coil's trace resistance, likely caused by skin effect at these frequencies. In a practical transceiver operating within a cellular infrastructure, a commonly used tradeoff is to strive to improve TX efficiency–since it limits battery life–at the expense of RX sensitivity. Accordingly we position the tap on the hybrid coil away from the center towards the ANT port so that in the equivalent circuit, $L_1=1.9$ nH, $L_2=3.8$ nH, and $M=1.8$ nH. This is more meaningful than to specify the location of the tap as a ratio of two non-integer numbers of turns. Then $L_1'=3.7$ nH and $L_2'=5.6$ nH, so the skew factor $k=1.5$.

Neglecting losses in the coil, (18) predicts that $\mathcal{G}_{avl}(\mathrm{TX}-\mathrm{ANT})=2.2$ dB and $F(\mathrm{ANT}-\mathrm{RX})=4$ dB. Full electromagnetic simulations that include metal and substrate losses and imperfect coupling between the coil segments show that these two quantities will be slightly worse, 2.5 dB and 4.6 dB, respectively. Substrate loss is kept low by constructing the coil in the uppermost layers of metal [27].

B. LNA Design

The antenna drives the duplexer at the ANT port through an ATU to correct for antenna impedance variations. The ATU is terminated by the driving point impedance (Z_{in}) at the duplexer's ANT port, with the TX and BAL ports terminated with the appropriate resistors and the RX port is terminated by a capacitance $C_{\rm RX}$.

The analysis of driving point impedance for the practical duplexer is straightforward enough, although it leads to slightly involved expressions. Using the relationships (4) and (13) it can be expressed in terms of the nominal antenna resistance $R_{\rm ANT}$. At the nominal center frequency of duplexer operation, the approximate driving point impedance is

$$Z_{in}\simeq\frac{k}{k+2}R_{\rm ANT} \tag{19}$$

where k is the skew factor of the tap on the coil, and no reactances appear because of their small contribution. Since we have chosen $k=1.5$, (19) leads to a reflection coefficient of 2/5 or -8 dB against a reference resistance of $R_{\rm ANT}$. While this may not be the ideal termination for the ATU, we believe it is good enough. We point out that Z_{in} is determined by resistors at the TX and BAL ports only, and not by the LNA input which is purely capacitive. The receiver's low noise amplifier (LNA) is the pseudo-differential common source circuit shown in Fig. 8, which avoids the 6 dB voltage loss in an impedance-matched LNA. But it adds 0.3 pF of capacitance between the ANT and BAL terminals and common. The duplexer connects to the antenna through an ATU, and to the PA through a lossless impedance matching network. $C_{\rm ATU}$ and C_{tune} can correct for inductive components in the antenna impedance, allowing the bridge network to balance with an on-chip network comprising switched resistors and capacitors, but no inductors.

C. Balancing Network and Narrowband RX Isolation

In the absence of parasitic reactances, the isolation in this duplexer depends solely on the resolution of the balancing impedance. For 50 dB isolation, roughly a 0.3 Ω resolution is needed. According to (13), $R_{\rm BAL}$ is nominally 80 Ω to balance a 50 Ω antenna impedance. To account for post-ATU variations

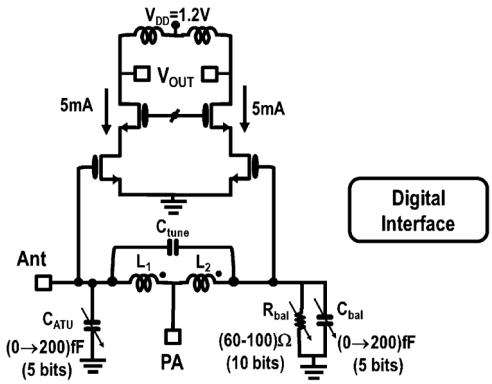

Fig. 8. Simplified schematic of the prototype chip.

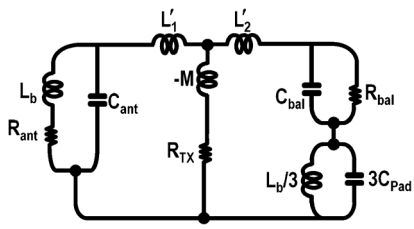

Fig. 9. Equivalent circuit, including parasitic inductances, L_b represents bondwire, $L_b/3$ is three downbonds to ground.

in antenna impedance as well as spreads in fabrication, we need a variable resistor that spans 60 to 100 Ω with a step of less than 0.3 Ω. This is realized as a 10-bit array of switched resistors in parallel with unit size of 1 kΩ. Common-centroid layout lowers differential nonlinearity in resistance increments. The variable capacitor $C_{\rm BAL}$ ranges from 0 to 200 fF.

To achieve the range and resolution requirements at 2 GHz, the switch figure-of-merit, defined as the product of its ON resistance and its OFF capacitance, should be less than 1.2 ps. In 65 nm CMOS this figure is 0.5 ps for FETs of minimum channel length, and in 40 nm CMOS it is 0.36 ps. This figure-of-merit always improves with technology scaling.

If the antenna and balancing networks were each completely described by a shunt GC branch, then once balance is achieved it will hold over a very wide bandwidth. However the antenna displays a complex and unpredictable impedance which is controlled by the ATU to some degree. This will be balanced by the on-chip digitally controlled shunt GC network, which connects through three bondwires in parallel to off-chip ground (Fig. 9).

If we assume that the antenna is represented by a pure 50 Ω as, for instance, during measurements on a network analyzer, then bondwire inductors (each roughly 1 nH) should be included as parasitics, which means that the topologies of the networks at the ANT and BAL ports are no longer the same. Consequently balancing, according to (17), becomes narrowband. For example, if a -50 dB rejection to RX is being sought, the expressions for admittance when substituted into (17) predict that this rejection will be available in ± 140 MHz around a null centered at 2 GHz. Measurements are close to this value, and the isolation bandwidth is good enough for our use.

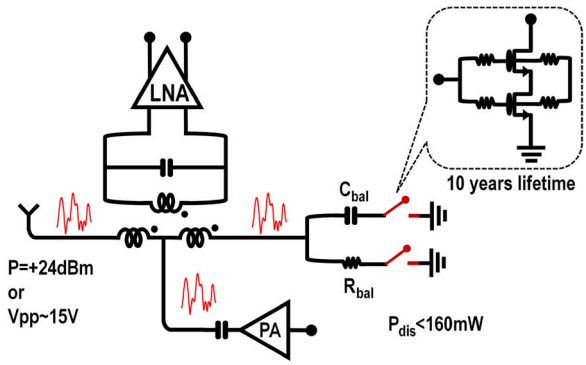

Fig. 10. Full power support in the CMOS integrated duplexer.

D. Full Power Support

The 3G standard specifies a maximum output power level of +24 dBm at the antenna. A modulation with a typical peak-to-average ratio of 3.2 dB will induce 15 V peak-to-peak swing at the antenna. In our prototype duplexer based on the autotransformer, the power amplifier would drive each terminal of the RX port relative to ground with this voltage swing, which would cause breakdown in the LNA FETs if they are of minimum channel length. However, a duplexer based on a two coil hybrid transformer (Fig. 4(c)) would protect the LNA FETs because this high voltage appears in common-mode at the primary coil, and ideally it is rejected at the secondary coil. At the time of this work, the effort involved in the design of a two layer transformer posed an unacceptable design risk.

Since our demonstrations of initial feasibility [16], [28], another work [29] reports duplexer operation at the full PA power level of +27 dBm. This duplexer employs a fully-differential version of the hybrid transformer of Fig. 4(c) to reject TX-to-RX common-mode voltage, although the two spirals stacked on different metal layers will couple capacitively. It handles a full 15 V using tradeoffs in the balance network. Properly designed inductors, capacitors, and resistors can tolerate this swing [29]. The 160 mW dissipated in the balance resistor under this extreme condition is well within the capacity of a simple heat sink. However the CMOS switches in the balance network are vulnerable to breakdown (Fig. 10), since for best figure-of-merit they must be short-channel devices. FETs stacked in a floating well structure [30] or on a sapphire substrate [31] can sustain large voltages; for example, in 65 nm CMOS a stack of two thick-oxide switches with an AC-floating body can tolerate the 15 V swing reliably over 10 years of operation. A taller stack may be needed to protect from distortion due to nonlinear switch resistance. We believe a full-power duplexer should be co-designed with the PA to exploit built-in impedance transformations to their fullest.

The prototype presented here is limited to moderate signal voltages, because its object was to show that tunable isolation over a wide band is practically achievable without sacrificing RX noise figure. The switches were built with thin-oxide FETs, and the LNA was connected directly to the autotransformer [28] (Fig. 8) without mediation of a magnetically-coupled second coil.

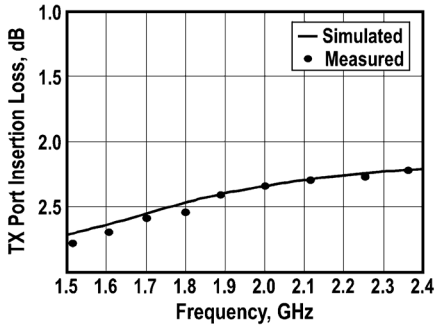

Fig. 11. Measured TX port insertion loss.

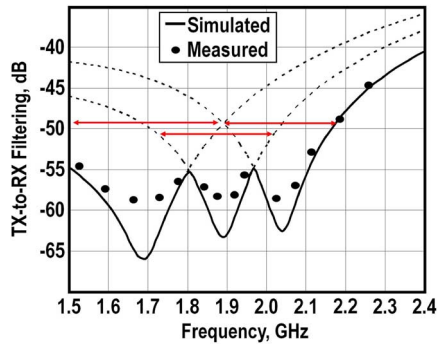

Fig. 12. Measured TX-to-RX isolation.

VI. Measurement Results

The duplexer plus LNA was characterized on a network analyzer that measures s-parameters against a 50 Ω reference. *Insertion gain*, s_{21}, is the transducer gain when the source and load resistances are *both* equal to this reference [18], [19]. At the TX port, a matching network on the PC board that includes bondwire and pad reactances transforms the instrument's 50 Ω to 35 Ω. The measured TX insertion loss $(1/s_{21})$ for WCDMA Band I, shown in Fig. 11, is only slightly lower than the simulated 2.5 dB.

Fig. 12 shows the isolation as the composite response for three balance settings as the duplexer is tuned across five 3G bands. Measured isolation exceeds 50 dB over more than 200 MHz of bandwidth, as predicted by simple analysis on an accurate equivalent circuit (see end of Section V-C). Fig. 13 plots the measured noise figure and gain for the cascade of the duplexer and LNA in the receive path. The in-band noise figure (referred to a 50 Ω source) is about 5 dB, accounted for by the loss in the termination resistors of the duplexer coil alone. The LNA FETs contribute little to the total noise. This illustrates the benefits of connecting the LNA FETs directly to the RX port, without transforming their input capacitance into a resistance. After the loading at the network analyzer's sensing port is de-embedded, the insertion gain ranges from 25 to 30 dB. Each curve corresponds to a specific setting of the LNA load. The return loss at the ANT port, measured while the TX port is terminated in 50 Ω, is better than 8 dB across the band of interest (Fig. 14). This value is predicted following equation (19). The reasonably well-matched input impedance terminates the antenna tuning unit.

The detailed performance of the duplexer and LNA is summarized in Table I. It is compared with a state-of-the art off-chip commercial SAW duplexer, and includes an additional loss of 1.2 dB arising from the RF switch and from connections to the PCB traces. The off-chip duplexer arrangement will show a total TX insertion loss of 3.2 dB. Our integrated duplexer suffers a TX loss of 2.5 dB. This 0.7 dB difference brings the same benefits as improving the PA efficiency by 15%. The isolation of the integrated duplexer is superior to the off-chip duplexer in both TX and RX bands, and it has a lower noise figure in the receive direction. The integrated duplexer covers five bands and is built on the transceiver chip, freeing up valuable board space.

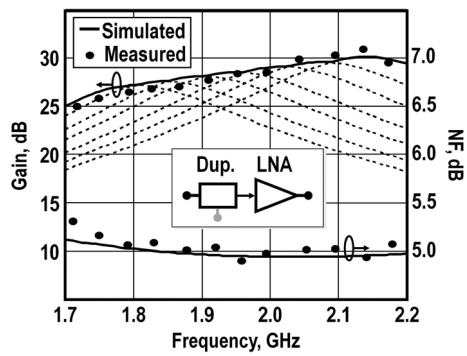

Fig. 13. Measured gain and NF of the cascaded duplexer and LNA.

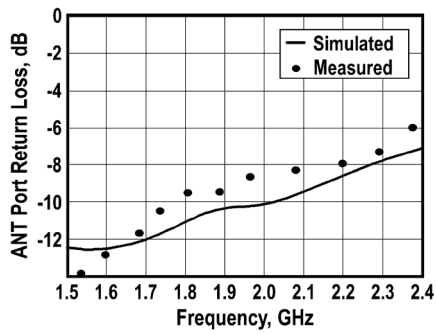

Fig. 14. Measured antenna return loss.

TABLE I
Performance of the Integrated Duplexer Compared With Off-Chip Discrete Duplexer

Parameter	Off-chip Duplexer‡	This Work
Duplexer TX IL	1.2^a+2^b= 3.2dB	2.5dB
Isolation in TX band	50dB	>50dB
Isolation in RX band	45dB	>45dB
Cascaded RX NF	$1.2^a+2.6^b+2^c$= 5.8dB	5.0dB
Gain	--	>26dB
Bands Covered	I	I,II,III,IV,IX
Area	7.5mm^2	0.2mm^2

VII. Discussion on Varying Antenna Impedance

Since this duplexer's isolating action depends on bridge balance, then to remain useful in a mobile device it must track changes in antenna impedance and continuously adjust the balancing network as the device moves in its environment (also

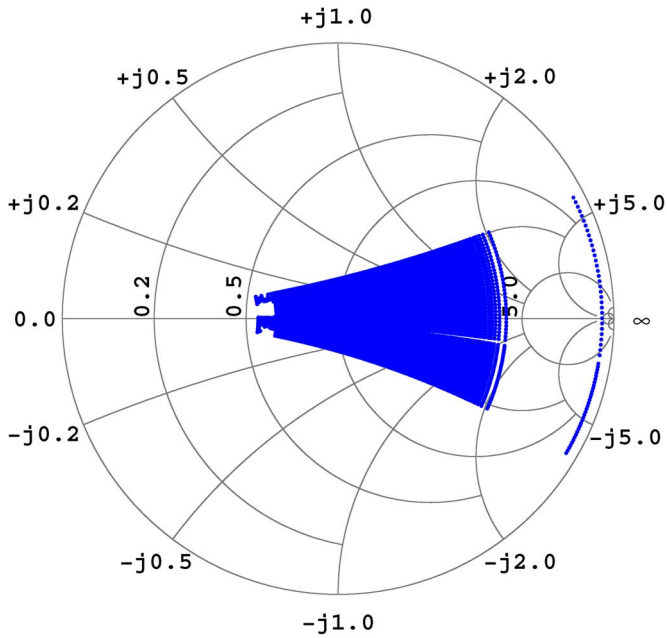

Fig. 15. The acceptable impedance range at the ANT port that can be balanced for 45 dB isolation, inductive reactances tuned by C_{ANT}, the balance network of Fig. 8 adjusted at each impedance for best performance.

called "user interaction"). This is a complex problem which entails taking measurements on electrically short antennas in realistic use scenarios, developing real-time tracking algorithms, and almost certainly depending on a variable ATU to tame the large fluctuations in antenna impedance. When the ATU confines VSWR to, say, less than 2:1, it brings the dual benefit of more efficient use of the power amplifier and of satisfactory duplexing with a simple balance network. However it was well outside our own capabilities to characterize the spreads of user interactions, so instead we rely on published data. [26] describes a production ATU and the results of experiments on actual mobile phone antennas across a range of realistic user interactions. The ATU is tuned by a real-time adaptation algorithm implemented on an embedded microcontroller. Experimental results show that the ATU can, in practice, confine the VSWR to about 2:1. This is referred to as the "matching domain" on the Smith Chart.

The question now is whether our prototype duplexer with its simple balance network can work to specification within this ATU domain. To investigate this, we plot on the Smith Chart in Fig. 15 the full span of impedances at the ANT port that can be balanced sufficiently to obtain 45 dB isolation from TX to RX. This span overlaps the matching domain of the ATU cited above [26] reasonably well. The inductive reactance at the ATU output is tuned by the on-chip C_{ANT} array.

On the other hand, as far as TX-to-RX isolation goes a duplexer based on SAW filters is largely immune to variations in antenna impedance, although an ATU may still be needed to improve the efficiency of power transfer from PA to antenna. While the SAW duplexer is robust in this respect, it is limited to a specific frequency band. By contrast, the duplexer presented in this paper is suitable for wideband use, but it depends on an ATU to encompass variations in antenna impedance. A sufficiently high order balance network could, in principle, assume the role of the ATU, but its on-chip realization is challenging. Since the ATU is also present in the receive path, its insertion loss will add to the cascade receive noise figure. An insertion loss of roughly 0.5 dB has been reported [32].

It is not clear at this point whether under all possible user interactions, this duplexer's isolation bandwidth is wide enough to span all possible receive bands.

VIII. Conclusion

We have presented the theory and design details of the first duplexer integrated on a CMOS chip that operates at 2 GHz. It is based on the hybrid autotransformer with a digitally-controlled balancing network. The measured performance of the CMOS duplexer suggests competitive performance with commercially available SAW duplexers, with the advantage of tunable wideband operation. However, to cover the very large ranges of antenna impedance seen in practical use scenarios, an adaptive antenna tuning unit must be employed. This work illuminates a promising path to replace today's band-specific duplexers constructed with SAW filters with a wideband device that can be fabricated on a CMOS chip.

References

[1] H. Darabi, A. Mirzaei, and M. Mikhemar, "Highly integrated and tunable RF front ends for reconfigurable multiband transceivers: A tutorial," *IEEE Trans. Circuits Syst. I: Reg. Papers*, vol. 58, no. 9, pp. 2038–2050, Sep. 2011.

[2] J. Kim, Y. Yoon, H. Kim, K. H. An, W. Kim, H.-W. Kim, C.-H. Lee, and K. T. Kornegay, "A linear multi-mode CMOS power amplifier with discrete resizing and concurrent power combining structure," *IEEE J. Solid-State Circuits*, vol. 46, no. 5, pp. 1034–1048, 2011.

[3] C. D. Presti, F. Carrara, A. Scuderi, P. M. Asbeck, and G. Palmisano, "A 25 dBm digitally modulated CMOS power amplifier for WCDMA/EDGE/OFDM with adaptive digital predistortion and efficient power control," *IEEE J. Solid-State Circuits*, vol. 44, no. 7, pp. 1883–1896, 2009.

[4] H. Darabi, "A blocker filtering technique for SAW-less wireless receivers," *IEEE J. Solid-State Circuits*, vol. 42, no. 12, pp. 2766–2773, Dec. 2007.

[5] A. Mirzaei, H. Darabi, A. Yazdi, Z. Zhou, E. Chang, and P. Suri, "A 65 nm CMOS quad-band SAW-less receiver SoC for GSM/GPRS/EDGE," *IEEE J. Solid-State Circuits*, vol. 46, no. 99, pp. 950–964, Apr. 2011.

[6] C. W. Zabel, "Balanced duplexers," in *Microwave Duplexers*, ser. MIT Radiation Lab, L. D. Smullin and C. G. Montgomery, Eds. New York, NY, USA: McGraw-Hill, 1948, vol. 14.

[7] H. J. Carlin and A. B. Giordano, *Network Theory*. Englewood Cliffs, NJ, USA: Prentice-Hall, 1964.

[8] V. Aparin, G. Ballantyne, C. Persico, and A. Cicalini, "An integrated LMS adaptive filter of TX leakage for CDMA receiver front ends," *IEEE J. Solid-State Circuits*, vol. 41, no. 5, pp. 1171–1182, 2006.

[9] N. Kamogawa, S. Dokai, N. Shibagaki, M. Hikita, T. Shiba, S. Ogawa, S. Wakamori, K. Sakiyama, T. Ide, and N. Hosaka, "Miniature SAW duplexers with high power capability," in *Proc. IEEE Ultrasonics Symp.*, 1998, vol. 1, pp. 119–122.

[10] M. Hikita, K. Sakiyama, O. Hikino, and M. Kijima, "New low-distortion band-switching techniques for SAW antenna duplexers used in ultra-wide-band cellular phone," *IEEE Trans. Microw. Theory Tech.*, vol. 52, no. 1, pp. 38–45, 2004.

[11] G. Campbell and R. Foster, "Maximum output networks for telephone substation and repeater circuits," *Trans. AIEE*, vol. 39, pp. 231–280, 1920.

[12] E. Sartori, "Hybrid transformers," *IEEE Trans. Parts, Mater. Packag.*, vol. 4, no. 3, pp. 59–66, 1968.

[13] M. D. Balkovich, H. J. Bouma, R. Carlson, D. C. Franke, W. G. Heffron, F. G. Oram, K. J. Pfeffer, P. T. Porter, S. P. Shramko, and R. W. Stubblefield, "Customer-services equipment and systems," in *Engineering and Operations in the Bell System*, R. F. Rey, Ed. Murray Hill, NJ, USA: AT&T Bell Labs, 1983.

[14] H. O. Friedheim, "On hybrid transformers," *A.T.E. Journal*, vol. 14, no. 3, pp. 218–228, 1958.

[15] H. A. M. Clark and P. B. Vanderlyn, "Double-ratio a.c. bridges with inductively-coupled ratio arms," *Proc. IEE—Part III: Radio and Communication Engineering*, vol. 96, no. 41, pp. 189–202, 1949.

[16] M. Mikhemar, H. Darabi, and A. Abidi, "A tunable integrated duplexer with 50 dB isolation in 40 nm CMOS," in *2009 IEEE Int. Solid-State Circuits Conf. (ISSCC) Dig. Tech. Papers*, San Francisco, CA, USA, Feb. 2009, pp. 386–387, 387a.

[17] P. Pursula and H. Seppä, "Hybrid transformer-based adaptive RF front end for UHF RFID mobile phone readers," in *Proc. IEEE Int. Conf. RFID*, Las Vegas, NV, USA, 2008, pp. 150–155.

[18] R. Gilmore and L. Besser, *Practical RF Circuit Design for Modern Wireless Systems: Passive Circuits and Systems*. Boston, MA, USA: Artech House, 2003, vol. 1.

[19] R. W. Anderson, "S-Parameter Techniques for Faster, More Accurate Network Design," Hewlett Packard, Application Note 95–1, 1995.

[20] H. T. Friis, "Noise figures of radio receivers," *Proc. IRE*, vol. 32, no. 7, pp. 419–422, 1944.

[21] C. Desoer and E. Kuh, *Basic Circuit Theory*. New York, NY, USA: McGraw-Hill, 1969.

[22] K. Boyle, Y. Yuan, and L. Ligthart, "Analysis of mobile phone antenna impedance variations with user proximity," *IEEE Trans. Antennas Propag.*, vol. 55, no. 2, pp. 364–372, 2007.

[23] M. E. Van Valkenburg, *Network Analysis*. Englewood Cliffs, NJ, USA: Prentice-Hall, 1974.

[24] Y. Sun and J. K. Fidler, "High-speed automatic antenna tuning units," in *Proc. 9th Int. Conf. Antennas and Propagation*, 1995, vol. 1, pp. 218–222.

[25] Y. Sun, J. Moritz, and X. Zhu, "Adaptive impedance matching and antenna tuning for green software-defined and cognitive radio," in *Proc. IEEE Int. Midwest Symp. Circuits and Systems*, 2011, pp. 1–4.

[26] K. R. Boyle, E. Spits, M. A. De Jongh, S. Sato, T. Bakker, and A. Van Bezooijen, "A self-contained adaptive antenna tuner for mobile phones: Featuring a self-learning calibration procedure," in *Proc. 6th European Conf. Antennas and Propagation*, 2012, pp. 1804–1808.

[27] A. Niknejad and R. Meyer, "Analysis, design, and optimization of spiral inductors and transformers for Si RF ICs," *IEEE J. Solid-State Circuits*, vol. 33, no. 10, pp. 1470–1481, Oct 1998.

[28] M. Mikhemar, H. Darabi, and A. Abidi, "An on-chip wideband and low-loss duplexer for 3G/4G CMOS radios," in *Proc. IEEE Symp. VLSI Circuits*, 2010, pp. 129–130.

[29] S. H. Abdelhalem, P. S. Gudem, and L. E. Larson, "A tunable differential duplexer in 90 nm CMOS," in *Proc. IEEE Radio Frequency Integrated Circuits Symp.*, Montreal, Canada, 2012, pp. 101–104.

[30] M. Ahn, H. Kim, C. Lee, and J. Laskar, "A 1.8-GHz 33-dBm P 0.1-dB CMOS T/R switch Using stacked FETs with feed-forward capacitors in a floated well structure," *IEEE Trans. Microw. Theory Tech.*, vol. 57, no. 11, pp. 2661–2670, 2009.

[31] R. B. Whatley, T. Ranta, and D. J. Kelly, "CMOS based tunable matching networks for cellular handset applications," in *IEEE Microwave Symp. Dig.*, 2011.

[32] M. De Jongh, A. Van Bezooijen, K. Boyle, and T. Bakker, "Mobile phone performance improvements using an adaptively controlled antenna tuner," in *IEEE Microwave Symp. Dig.*, 2011.

Mohyee Mikhemar (M'08) received the B.S. and M.S. degrees with honors in electrical engineering from Ain Shams University, Egypt, in 2000 and 2004, respectively. He received the Ph.D. degree from the University of California, Los Angeles (UCLA), CA, USA, in 2009.

He has been with Broadcom Corporation, Irvine, CA, USA, since 2007. He is currently a Principal Scientist at the advanced RF research and development group at Broadcom working on the design of the next generation low power and multi-band radios. His research interests include low power multi-band radio design in CMOS, tunable duplexers and RF filters on Silicon and digitally-assisted RF circuits.

Dr. Mikhemar has 41 issued/pending patent applications in the field of RF-CMOS design. He received the 2013 Jack Kilby award for outstanding student paper at ISSCC, the distinguished-technical-paper award from the ISSCC in 2012, UCLA Office of the Dean Fellowship (2008), UCLA EE Department Academic Excellence Fellowship (2006), UCLA Graduate Division Fellowship (2004), and the Egyptian Government Excellence Award (1995-2000).

Hooman Darabi (SM'05) was born in Tehran, Iran, in 1972. He received the B.S. and M.S. degrees both in electrical engineering from Sharif University of Technology, Tehran, Iran, in 1994 and 1996, respectively. He received the Ph.D. degree in electrical engineering from the University of California, Los Angeles, CA, USA, in 1999.

He is currently a Sr. Technical Director, and a Fellow, with Broadcom Corporation, Irvine, CA, within the RF group in Mobile and Wireless Business Unit. His interests include analog and RF IC design for wireless communications. He holds over 200 issued or pending patents with Broadcom, and has published over 50 peer reviewed or conference papers. He is an IEEE distinguished lecturer.

Asad A. Abidi (F'96) received the B.Sc. degree (with honors) from Imperial College, London, U.K., in 1976, and the M.S. and Ph.D. degrees in electrical engineering from the University of California, Berkeley, CA, USA, in 1978 and 1981, respectively.

From 1981 to 1984, he was with Bell Laboratories, Murray Hill, NJ, USA, as a Member of the Technical Staff with the Advanced LSI Development Laboratory. Since 1985, he has been with the Electrical Engineering Department, University of California, Los Angeles, CA, USA, where he is Chancellor's Professor. He was a Visiting Faculty Researcher with Hewlett-Packard Laboratories in 1989. His research interests include RF CMOS design, high-speed analog integrated circuit design, data conversion, and other methods of analog signal processing.

Dr. Abidi is a member of the U.S. National Academy of Engineering and Associate Fellow of TWAS-the science academy of the developing world. From 1992 to 1995, he was an Editor for the IEEE JOURNAL OF SOLID-STATE CIRCUITS. He received an IEEE Millennium Medal, the 1988 TRW Award for Innovative Teaching, the 1997 IEEE Donald G. Fink Award, the 2007 Lockheed-Martin Award for Excellence in Teaching, and the 2008 IEEE Solid-State Circuit Society's Donald O. Pederson Award. He was named one of the top ten contributors to the ISSCC in its 50 years.